IMA Journal of Applied Mathematics (2012) **77**, 196–219
doi:10.1093/imamat/hxr017
Advance Access publication on March 23, 2011

Three flow regimes of viscous jet falling onto a moving surface

A. HLOD*, A. C. T. AARTS, A. A. F. VAN DE VEN AND M. A. PELETIER
Center for Analysis, Scientific computing and Applications,
Eindhoven University of Technology, 5600 MB Eindhoven,
The Netherlands

*Corresponding author: avhlod@gmail.com

[Received on 6 December 2010; revised on 6 December 2010;
accepted on 21 February 2011]

A stationary viscous jet falling from an oriented nozzle onto a moving surface is studied theoretically. The fluid is modelled as a Newtonian fluid, and the model for the flow includes viscous effects, inertia and gravity. We distinguish three flow regimes, called *inertial, viscous-inertial* and *viscous*, according to which effect is dominant in the momentum transfer through the jet cross section. By studying the characteristics of the conservation of momentum for a dynamic jet, the boundary conditions for each flow regime are derived, and the flow regimes are characterized in terms of the process and material parameters. The model is solved by a transformation into an algebraic equation. The parameter regions of the three flow regimes, and their boundaries, are confirmed experimentally. Influences of surface tension, bending stiffness and air drag are presented.

Keywords: viscous jet; moving surface.

1. Introduction

During the fall under gravity of a viscous jet from an oriented nozzle onto a moving surface, called the belt, three flow regimes can be observed. In this paper, we characterize the three regimes by the dominant effect in the momentum transfer through the jet cross section providing us the classification *inertial*, *viscous-inertial* or *viscous* and simultaneously by the convexity of the jet shape (concave, straight vertical and convex). As we will show, the convexity of the jet shape is related to the dominant effect in the momentum transfer.

In the first flow regime, the jet shape is concave, apart from a boundary layer at the belt and aligned with the nozzle orientation and resembles a ballistic trajectory; see Fig. 1(a and b). We call this flow regime as *inertial* and the associated jet as an *inertial jet* because the inertia dominates in the momentum transfer through the jet cross section. The inertial jet occurs for large flow velocity at the nozzle with respect to the velocity of the belt and small viscosity.

The jet in the second flow regime has a straight, vertical shape, apart from boundary layers at the nozzle and at the belt; see Fig. 1(c). We call this flow regime *viscous-inertial*, and the associated jet a *viscous-inertial jet* because the viscosity dominates at the nozzle and inertia at the belt. The viscous-inertial jet happens for large falling heights, large viscosity and intermediate values of the flow velocity at the nozzle with respect to the velocity of the belt.

In the third flow regime, apart from a boundary layer at the nozzle, the jet shape is convex, and the jet touches the belt tangentially; see Fig. 1(d). This flow regime we call *viscous*, and the associated jet a

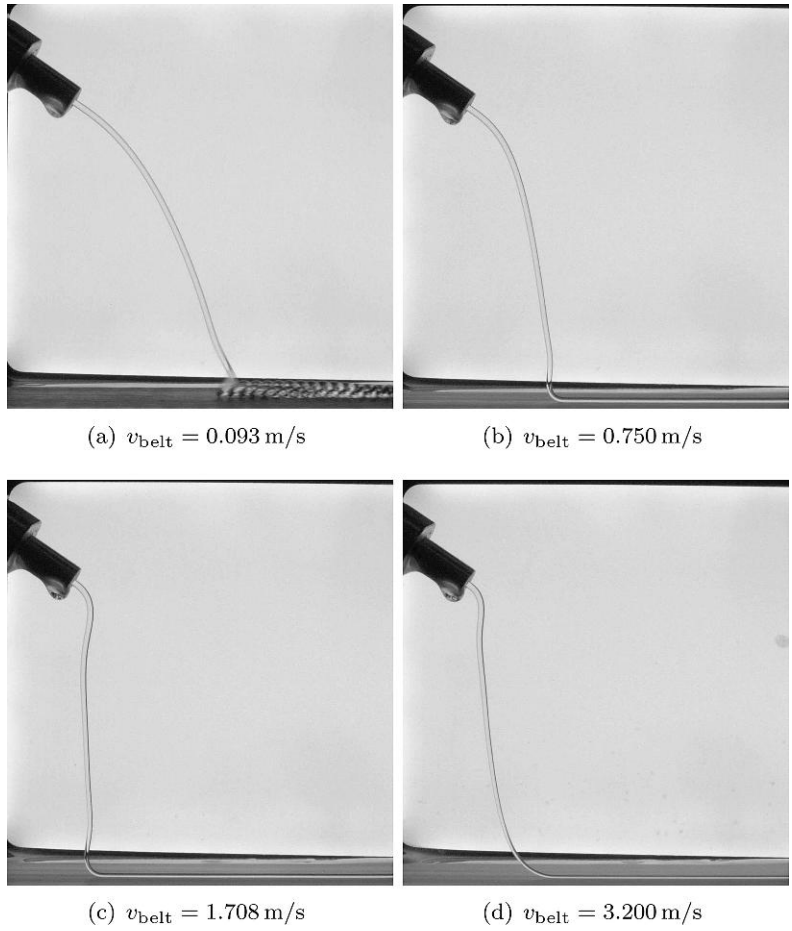

FIG. 1. Typical jet shapes. The belt, shown at the bottom of the images, moves from left to right. The jet shape changes from concave (Fig. 1(a and 1b)) to vertical (Fig. 1(c)), and from vertical to convex (Fig. 1(d)), as the belt velocity v_{belt} is increased. Parameters are given in Table 1 under Sequence 2.

viscous jet[1] because the viscosity dominates in the momentum transfer. The viscous jet occurs for high fluid viscosity, small velocity at the nozzle with respect to the velocity of the belt, and small falling height.

In this paper, we address the characterization of the three flow regimes. For this, we choose a 'string model,'[2] in which the jet has no resistance to bending. We will determine when and how the system parameters, such as the nozzle and belt orientations and velocities, influence the jet shape and investigate the capabilities and limitations of this jet model. This work should be seen as a continuation and generalization of our previous publication on the regime that we now call viscous jet (Hlod *et al.*, 2007).

[1]The term 'viscous jet' is often used to indicate that the fluid in the jet is viscous, and that the viscosity plays an important role. In the current setup, we prefer to use the term 'viscous' to indicate that the viscosity is the dominant force in the momentum transfer.

[2]This name for the jet model is used because of the analogy to elastic strings; see Marheineke & Wegener (2009).

The fall of jets or sheets of viscous fluids from a nozzle oriented vertically down onto a *fixed* surface has been widely studied. Here, one can observe unstable behaviour such as coiling for round jets and folding for planar sheets; see, for example, Taylor (1969), Skorobogatiy & Mahadevan (2000), Yarin & Tchavdarov (1996), Ribe (2003, 2004), Cruickshank (1980) and Tchavdarov *et al.* (1993). Vertically falling jets have been studied theoretically and experimentally in Clarke (1966, 1968), Adachi (1987) and Sauter *et al.* (2005). Experimental investigations of steady and unsteady flows of jets falling under gravity onto a *moving* surface from a vertical nozzle were presented in Chiu-Webster & Lister (2006), Ribe *et al.* (2006), Hlod *et al.* (2007) and Morris *et al.* (2008).

Chiu-Webster & Lister (2006) experimentally study the same set-up as in this paper, only considering a nozzle pointing vertically downwards, and concentrating on the resulting rich variety of patterns laid down by the jet. The patterns are characterized and parameter regions for each pattern are found experimentally. In the second, theoretical, part of (Chiu-Webster & Lister, 2006) the curved steady jet (viscous in our classification) is modelled using a similar string model that also includes surface tension. The model equations have been solved only for a subset of the admissible parameter space. In Hlod *et al.* (2007), we showed that for the jet model of Chiu-Webster & Lister (2006), but without surface tension, a solution exists only in a subset of the parameter space; we conjecture that the same holds for the model with surface tension, and this is corroborated by numerical evidence in Chiu-Webster & Lister (2006).

In other work, varying nozzle angles are considered, e.g. Marheineke & Wegener (2009), Panda (2006); Panda *et al.* (2008), Wallwork *et al.* (2002), Parau *et al.* (2006, 2007), Decent *et al.* (2002), Uddin *et al.* (2006), Partridge *et al.* (2005) and Wong *et al.* (2004). In all these publications, it is assumed that the jet orientation at the nozzle is aligned with the nozzle orientation. However, a solution for a string jet model with the jet aligned with the nozzle may not exist as is shown in Götz *et al.* (2008).

At this point, three natural questions arise, namely why does a solution for the string jet model not exist for all parameter values, what can be done to obtain a jet solution outside the existence parameter regions presented in Chiu-Webster & Lister (2006), Hlod *et al.* (2007) and Götz *et al.* (2008), and what is the role of the assumption of alignment at the nozzle or the belt? We answer these questions by developing a model that fully describes the three flow regimes. For the jet, we use a model that includes effects of inertia, viscosity and gravity but neglects surface tension, bending stiffness and air drag. The fluid is considered to be incompressible, isothermal and Newtonian. We allow the nozzle orientation to vary between horizontal and vertically down. By studying the characteristics of the equation of conservation of momentum, we determine the parameter regions for each flow regime. Consideration of the characteristics as being the directions of information propagation explains why and when each of the three flow regimes occurs and gives the correct boundary conditions for each flow regime. The model presented in this paper can also be used to describe the fall of sheets onto a moving surface (curtain coating) (see Dyson *et al.*, 2005; Marston *et al.*, 2006, 2008).

We also confirm the existence of the three flow regimes experimentally. A comparison of the touchdown points with the belt for different belt velocities, while keeping the rest parameters fixed, allows us to indicate the regions of the three flow regimes. We also compare the jet shapes obtained experimentally and theoretically, which reveals substantial differences. Including either surface tension, or bending stiffness, or air drag alone does not explain the shapes mismatch. Suggestions are made how to change the model and experimental setup to get a better jet shapes agreement.

The structure of the paper is as follows. The background of the problem is presented in Section 2. In Section 3, the model equations are derived and simplified to a first-order differential equation on an unknown domain. The analysis of the characteristics of the conservation of momentum equation for dynamic jets in order to derive correct boundary conditions is done in Sections 4 and 5, and in Section 6, the results from the model are presented. Experiments confirming existence of the three flow regimes

and comparison with the theory are presented in Section 7. The characteristic features of the three flow regimes are summarized in Section 8, and conclusions are made in Section 9.

2. Background of the problem

The motivation for this study came from an industrial application of rotary spinning of aramid fibers. Here, we briefly describe the rotary spinning process. For a detailed description, we refer to Hlod (2009), Kolk (2005) and den Decker *et al.* (2004).

The rotary spinning setup consists of two cylinders. The smaller one (the *rotor*) is placed inside the larger one (the *coagulator*), so that their axes are vertical and coincide (Fig. 2). The rotor is filled with the fluid, a polymer solution, and is rotated while the coagulator is fixed. The polymer solution is forced through nozzles in the lateral surface of the rotor and moves as a jet towards the coagulator where it is captured by a water curtain.

The first published model of rotary spinning was in den Decker *et al.* (2004). There the jet between the rotor and the coagulator was described using the effects of extensional viscosity, inertia and centrifugal and Coriolis forces; gravity, air drag, surface tension, viscoelasticity, bending resistance and thermal effects were neglected. It was assumed that the jet leaves the nozzle of the rotor radially and that the fluid is Newtonian. In such a way one obtains a simple jet model in 2D (the horizontal plane) that gives some insight into the rotary spinning. However, this model did not produce a satisfactory solution for the actual process parameters —(see den Decker *et al.*, 2004). Experiments show that the jet orientation at the rotor is not always radial and depends on the process parameters.

A second step was done in Kolk (2005) where, based on visual observations, the assumption that the jet leaves the nozzle radially was dropped. Using further, the same model as den Decker *et al.* (2004) did, Kolk obtained a solution in which the jet orientation at the nozzle is not radial and depends on the process parameters.

However, the mechanisms determining the angle at which the jet leaves the rotor were not understood. In this paper, we use the same model for the jet but change the setup to a simpler and more

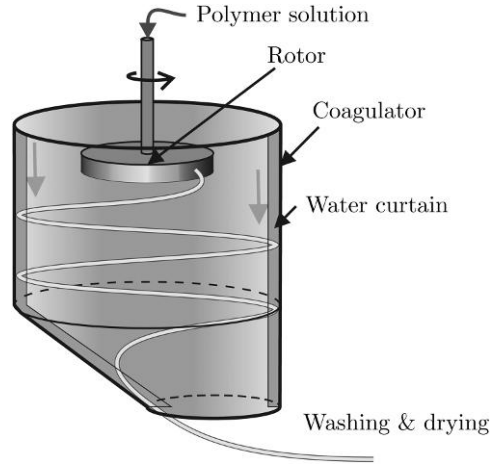

FIG. 2. A rotary spinning process. This setup provided the original motivation for the simpler setup of this paper and is studied in Hlod (2009).

accessible one, the jet falling onto a moving belt under gravity. The more complex problem of rotary spinning is discussed in Hlod (2009), where the same jet model is used.

3. Modelling

In this section, we present the model of a viscous jet falling onto a moving belt. To model the flow, we use a thin-jet approximation (a string model) and include effects of inertia, viscous extension and gravity. We assume the fluid to be incompressible, isothermal and Newtonian. We neglect surface tension, bending resistance and air drag; therefore any bending or buckling boundary layers at the nozzle or at the belt are disregarded. The jet is described by the equations of conservation of mass and momentum. First, we formulate the equations for the dynamic jet, which are used in Section 5 to justify our choice of boundary conditions. Next, we partly solve the steady jet equations and make an analysis showing that only three possible situations for the balance of the momentum transfer through the jet cross section can exist: inertial, viscous-inertial and viscous. Finally, we reformulate the problem by deriving an equivalent algebraic equation which is convenient for further analysis.

The jet is modelled as a curve in the x, z-plane of unknown length s_{end} (see Fig. 3). The curve is parameterized by its arc length s, with the origin $s = 0$ at the nozzle and $s = s_{\text{end}}$ at the touchdown point at the belt. The position of a certain point s of the jet at time t is described by its position vector $\mathbf{r} = \mathbf{r}(s, t)$ with respect to the origin 0, which is chosen at the nozzle point.

Figure 3 shows various geometric parameters. A local coordinate system is constructed at each point of the jet with as basis vectors the tangent and normal vectors $\mathbf{e}_t$ and $\mathbf{e}_n$. The angle between the tangent vector and horizontal direction is Θ, the horizontal distance between the nozzle and the touchdown point at the belt is x_{end}, and the flow velocity at a point s of the jet is $v = v(s, t)$. At the touchdown point, the jet has the same velocity as the belt v_{belt}, and the flow velocity at the nozzle is v_{nozzle}.

The system of equations describing a thin dynamical jet in 2D can be found in variety of publications, e.g. Roos *et al.* (1973), Yarin (1993) and Entov & Yarin (1980). It consists of the laws of conservation of mass and momentum

$$\mathcal{A}_t + (\mathcal{A}v)_s = 0, \tag{3.1}$$

$$\rho\mathcal{A}(\mathbf{r}_{tt} + \mathbf{r}_s(v_t + vv_s) + v^2\mathbf{r}_{ss} + 2v\mathbf{r}_{st}) = P_s\mathbf{r}_s + P\mathbf{r}_{ss} + \mathbf{K}', \tag{3.2}$$

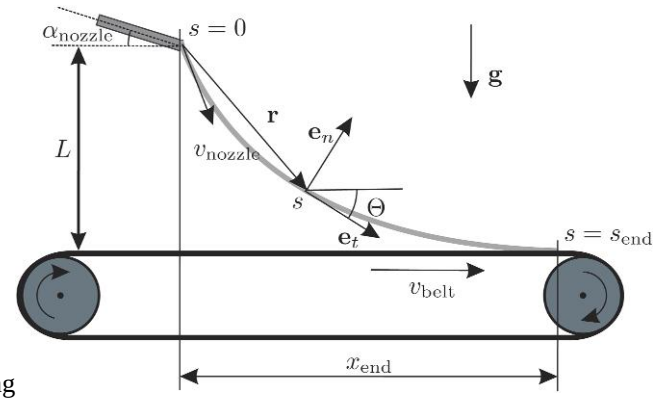

centering

FIG. 3. Model of a fall of a jet of viscous fluid onto a moving surface.

where $\mathcal{A} = \mathcal{A}(s,t)$ is the cross-sectional area, $P = P(s,t)$ the longitudinal force and $\mathbf{K}' = \mathbf{K}'(s,t)$ the external force per unit length of the jet. Subscripts denote differentiation. The longitudinal force P is given by a constitutive law, and in the case of a Newtonian viscous fluid, it is equal to

$$P = 3\nu\rho v_s \mathcal{A}. \tag{3.3}$$

Finally for $\mathbf{K}'$, we take

$$\mathbf{K}' = \rho \mathcal{A}\mathbf{g}, \tag{3.4}$$

the gravity force per unit of length of the jet (external air drag is neglected).

The stationary versions of (3.1) and (3.2) together with (3.3) and (3.4), and the condition for s as the arc length are

$$\mathcal{A}(\mathbf{r}_s v v_s + v^2 \mathbf{r}_{ss}) = 3\nu(v_s \mathcal{A}\mathbf{r}_s)_s + \mathcal{A}\mathbf{g}, \tag{3.5}$$

$$(\mathcal{A}v)_s = 0, \tag{3.6}$$

$$|\mathbf{r}_s| = 1. \tag{3.7}$$

Thus, we have three differential equations, (3.5–3.7), for the unknowns $\mathbf{r}$, v and $\mathcal{A}$. Next, we describe the boundary conditions.

For the velocity v, we prescribe two boundary conditions: at $s = 0$, the flow velocity at the nozzle is

$$v(0) = v_{\text{nozzle}}, \tag{3.8}$$

while at $s = s_{\text{end}}$, the jet sticks to the belt, so that

$$v(s_{\text{end}}) = v_{\text{belt}}. \tag{3.9}$$

The boundary condition for $\mathcal{A}$ follows form the known cross-sectional area of the nozzle as

$$\mathcal{A}(0) = \frac{\pi}{4} d^2_{\text{nozzle}}. \tag{3.10}$$

The fixed vertical distance between the nozzle and the belt gives the additional constraint

$$\int_0^{s_{\text{end}}} \sin\Theta(s)\mathrm{d}s = L. \tag{3.11}$$

To make the system (3.5–3.11) complete we need boundary conditions for $\mathbf{r}$. A well-known rule of thumb states that the second-order nature of (3.5) implies that two lateral boundary conditions for $\mathbf{r}$ are necessary and sufficient; however, as we shall show in Section 5, in this case, the situation is more subtle, and while one boundary condition is always necessary, whether or not the second condition is also required depends on the solution.

Since the position $\mathbf{r}$ is with respect to the fixed nozzle, we have one boundary condition for $\mathbf{r}$

$$\mathbf{r}(0) = \mathbf{0}. \tag{3.12}$$

The second boundary condition is chosen later in this section and is justified in Section 5. By integrating (3.6), using (3.8) and (3.10), we find that

$$\mathcal{A}(s) = \frac{F}{v(s)\rho},$$

where the mass flux is given by $F = \rho v_{\text{nozzle}} \pi d_{\text{nozzle}}^2/4$. We eliminate $\mathcal{A}$ from (3.5) to obtain

$$\mathbf{r}_s v_s + v\mathbf{r}_{ss} = 3\nu\left(\mathbf{r}_s \frac{v_s}{v}\right)_s + \frac{\mathbf{g}}{v}. \tag{3.13}$$

Next, we introduce a new variable ξ by

$$\xi = v - 3\nu\frac{v_s}{v}, \tag{3.14}$$

which represents the scaled momentum transfer through a jet cross section and plays a crucial role in our further analysis. By use of ξ, we write (3.13) as

$$(\xi \mathbf{r}_s)_s = \frac{\mathbf{g}}{v}. \tag{3.15}$$

Using $\mathbf{e}_t = \mathbf{r}_s$, and $(\mathbf{e}_t)_s = -\Theta_s \mathbf{e}_n$, we can write (3.15) in components as

$$\xi_s = \frac{g\sin(\Theta)}{v}, \tag{3.16}$$

and

$$\Theta_s = \frac{g\cos(\Theta)}{\xi v}. \tag{3.17}$$

Equation (3.17) requires a boundary condition for Θ; this is related to the question of boundary conditions for $\mathbf{r}$.

We now scale the system as follows: the length s is scaled with respect to $3\nu/v_{\text{nozzle}}$, and the velocity v with respect to v_{nozzle}. Then, (3.8), (3.9), (3.11), (3.14), (3.16) and (3.17) become

$$\xi_s = \frac{A\sin(\Theta)}{v}, \tag{3.18}$$

$$\Theta_s = \frac{A\cos(\Theta)}{\xi v}, \tag{3.19}$$

$$\xi = v - \frac{v_s}{v}, \tag{3.20}$$

$$v(0) = 1, \tag{3.21}$$

$$v(s_{\text{end}}) = \text{Dr}, \tag{3.22}$$

$$\int_0^{s_{\text{end}}} \sin(\Theta(s))\text{d}s = \text{Re}. \tag{3.23}$$

Here, $A = 3gv/v_{\text{nozzle}}^3$, $\text{Re} = v_{\text{nozzle}}L/(3\nu)$ is the Reynolds number, $\text{Dr} = v_{\text{belt}}/v_{\text{nozzle}}$ is the draw ratio, and the scaled s_{end} becomes $s_{\text{end}}v_{\text{nozzle}}/(3\nu)$. The dimensionless number A is related to the Froude number $\text{Fr} = v_{\text{nozzle}}/\sqrt{gL}$ and Re as $A = 1/(\text{ReFr}^2)$. After scaling, the system is described in terms of three positive dimensionless numbers, which define the parameter space $\mathscr{P}$ as

$$\mathscr{P} = \{(A, \text{Re}, \text{Dr}): A > 0, \text{Re} > 0, \text{Dr} > 0\}. \tag{3.24}$$

The nozzle orientation α_{nozzle} only appears in the boundary condition for Θ for the inertial jet, see (4.14) further on, and is considered to be fixed.

The system (3.18–3.23), describing stationary solutions, is the main mathematical problem of this paper.

4. Initial analysis and additional boundary conditions

By replacing the material coordinate s by the time variable τ, according to

$$\mathrm{d}s = v(\tau)\mathrm{d}\tau, \tag{4.1}$$

the system (3.18–3.23) becomes

$$\xi_\tau = A\sin(\Theta), \tag{4.2}$$

$$\Theta_\tau = \frac{A\cos(\Theta)}{\xi}, \tag{4.3}$$

$$\xi = v - \frac{v_\tau}{v^2}, \tag{4.4}$$

$$v(0) = 1, \tag{4.5}$$

$$v(\tau_{\mathrm{end}}) = \mathrm{Dr}, \tag{4.6}$$

$$\int_0^{\tau_{\mathrm{end}}} \sin(\Theta(\tau))v(\tau)\mathrm{d}\tau = \mathrm{Re}. \tag{4.7}$$

Here, τ_{end} is the result of the coordinate transformation (4.1) of $s_{\mathrm{end}} = \int_0^{\tau_{\mathrm{end}}} v(\tau)\mathrm{d}\tau$. Next, we solve (4.2) and (4.3), using the first integral

$$\xi\sin(\Theta) = A\tau + c_1 \tag{4.8}$$

to obtain

$$\xi = \pm\sqrt{A^2\tau^2 + 2Ac_1\tau + c_2}, \tag{4.9}$$

$$\Theta = \pm\arcsin\left(\frac{A\tau + c_1}{\sqrt{A^2\tau^2 + 2Ac_1\tau + c_2}}\right). \tag{4.10}$$

Here, c_1 and c_2 are constants to be determined later.

In the analysis, we restrict ourselves to solutions with $\Theta \in [0, \pi/2]$. We conclude from (4.2) that ξ is a strictly increasing function. Therefore, we distinguish three possible situations for the sign of ξ: always positive, a sign change from negative to positive and always negative, i.e.

$$0 < \xi(0) < \xi(\tau_{\mathrm{end}}), \tag{4.11}$$

$$\xi(0) \leqslant 0 \leqslant \xi(\tau_{\mathrm{end}}), \tag{4.12}$$

$$\xi(0) < \xi(\tau_{\mathrm{end}}) < 0. \tag{4.13}$$

If (4.11) holds, then it follows from (4.3) that Θ is a strictly increasing function implying that the jet has a concave shape. As will be justified in Section 5, we prescribe the nozzle orientation angle as the boundary condition for Θ, i.e.

$$\Theta(0) = \alpha_{\mathrm{nozzle}}. \tag{4.14}$$

Substitution of (4.14) into (4.9) and (4.10) gives

$$\xi = \sqrt{A^2\tau^2 + 2A\sqrt{c_2}\sin(\alpha_{\text{nozzle}})\tau + c_2}, \tag{4.15}$$

$$\Theta = \arcsin\left(\frac{A\tau + \sqrt{c_2}\sin(\alpha_{\text{nozzle}})}{\sqrt{A^2\tau^2 + 2A\sqrt{c_2}\sin(\alpha_{\text{nozzle}})\tau + c_2}}\right). \tag{4.16}$$

Because (4.11) implies that inertia dominates in the jet, we refer to a jet satisfying (4.11) as an inertial jet; as found above, the inertial jet has a concave shape.

For (4.12) to hold, there must exist a $\tau^* \in [0, \tau_{\text{end}}]$ such that $\xi(\tau^*) = 0$. Then from (4.3), it follows that $\Theta(\tau^*) = \pi/2$. Substituting τ^* into (4.10), we have

$$\frac{A\tau^* + c_1}{\sqrt{A^2(\tau^*)^2 + 2Ac_1\tau^* + c_2}} = 1, \tag{4.17}$$

giving $c_1^2 = c_2$. This implies that

$$\Theta \equiv \pi/2, \tag{4.18}$$

for all $\tau \in [0, \tau_{\text{end}}]$, and hence the jet is vertical, and

$$\xi = A\tau + c_1. \tag{4.19}$$

For ξ obeying (4.12), we obtain $\xi(\tau) = A\tau - \sqrt{(c_2)^2}$. Because (4.12) implies that the viscosity dominates at the nozzle and inertia at the belt, we refer to a jet satisfying (4.12) as a viscous-inertial jet. Hence, the viscous-inertial jet has a straight vertical shape. Note that for the viscous-inertial jet, as will be shown in Section 5, no boundary condition for Θ is necessary.

If (4.13) holds, then it follows from (4.3) that Θ is a strictly decreasing function. In this case, the jet has a convex shape. As will be justified in Section 5, we require tangency for the jet at the belt, i.e.

$$\Theta(\tau_{\text{end}}) = 0. \tag{4.20}$$

Then

$$\xi = -\sqrt{A^2\tau(\tau - 2\tau_{\text{end}}) + c_2}, \tag{4.21}$$

$$\Theta = \arcsin\left(\frac{A(\tau_{\text{end}} - \tau)}{\sqrt{A^2\tau(\tau - 2\tau_{\text{end}}) + c_2}}\right). \tag{4.22}$$

Because (4.13) implies that viscosity dominates everywhere in the jet we call a jet for which (4.13) holds a viscous jet, inferring that the viscous jet has a convex shape.

By substituting the found solutions for ξ and Θ into (4.4–4.7) for the three situations (4.11–4.13)

we obtain

$$v - \frac{v_\tau}{v^2} = \begin{cases} \sqrt{A^2\tau^2 + w^2 + 2A\tau w \sin(\alpha_{\text{nozzle}})} & \text{inertial jet,} \\ w + A\tau & \text{viscous-inertial jet,} \\ w\sqrt{A^2\tau(\tau - 2\tau_{\text{end}})/w^2 + 1} & \text{viscous jet,} \end{cases} \tag{4.23}$$

$$v(0) = 1, \tag{4.24}$$

$$v(\tau_{\text{end}}) = \text{Dr}, \tag{4.25}$$

$$\text{Re} = \begin{cases} \int_0^{\tau_{\text{end}}} \frac{A\tau + w\sin(\alpha_{\text{nozzle}})}{\sqrt{A^2\tau^2 + w^2 + 2A\tau w\sin(\alpha_{\text{nozzle}})}} v(\tau)\mathrm{d}\tau & \text{inertial jet,} \\ \int_0^{\tau_{\text{end}}} v(\tau)\mathrm{d}\tau & \text{viscous-inertial jet,} \\ \int_0^{\tau_{\text{end}}} \frac{A(\tau_{\text{end}} - \tau)}{\sqrt{A^2\tau(\tau - 2\tau_{\text{end}}) + w^2}} v(\tau)\mathrm{d}\tau & \text{viscous jet,} \end{cases} \tag{4.26}$$

where $w = \xi(0)$. We refer to the situations of inertial, viscous-inertial and viscous jets as inertial, viscous-inertial and viscous flow regimes, respectively.

For given $w \in \mathbb{R}$ and flow regime, the problem (4.23–4.25) has a solution $v(\tau; w)$ and $\tau_{\text{end}}(w)$, where $\tau_{\text{end}}(w)$ satisfies (4.25). Here, we assume that for any w, (4.25) has only one solution, which is not always true. However, this allows us to illustrate a solution procedure.

Substituting $v(\tau; w)$ and $\tau_{\text{end}}(w)$ into the integrals (4.26), we obtain the functions of w:

$$\begin{aligned} I_{\text{inert}}(w) &= \int_0^{\tau_{\text{end}}(w)} \frac{A\tau + w\sin(\alpha_{\text{nozzle}})}{\sqrt{A^2\tau^2 + w^2 + 2A\tau w\sin(\alpha_{\text{nozzle}})}} v_{\text{inert}}(\tau; w)\mathrm{d}\tau && \text{inertial jet,} \\ I_{\text{v-i}}(w) &= \int_0^{\tau_{\text{end}}(w)} v_{\text{v-i}}(\tau; w)\mathrm{d}\tau && \text{viscous-inertial jet,} \\ I_{\text{visc}}(w) &= \int_0^{\tau_{\text{end}}(w)} \frac{A(\tau_{\text{end}}(w) - \tau)}{\sqrt{A^2\tau(\tau - 2\tau_{\text{end}}(w)) + w^2}} v_{\text{visc}}(\tau; w)\mathrm{d}\tau && \text{viscous jet.} \end{aligned} \tag{4.27}$$

Here, we denote by $v_{\text{inert}}(\tau; w)$, $v_{\text{v-i}}(\tau; w)$ and $v_{\text{visc}}(\tau; w)$, the solution of (4.23) for a inertial, viscous-inertial and viscous jet, respectively. According to (4.11–4.13), $I_{\text{inert}}(w)$ is defined for $w > 0$, and $I_{\text{visc}}(w)$ and $I_{\text{v-i}}(w)$ for $w \leqslant 0$. With (4.27), solving (4.23–4.26) is equivalent to solving the algebraic equation

$$I_?(w) = \text{Re}, \tag{4.28}$$

where ? stands for an unknown jet flow regime. Therefore, a study of existence and uniqueness of a jet solution results into a study of the existence and uniqueness of a solution to the algebraic equation (4.28).

At this point, we briefly recapitulate the main steps in our solution procedure. We do this for the inertial flow; the other cases are analogous. The steps are

1. Solve $v = v_{\text{inert}}(\tau; w)$ from $(4.23)_1$, with use of the boundary condition (4.24).
2. Find $\tau_{\text{end}}(w)$ from (4.25) as $v_{\text{inert}}(\tau_{\text{end}}(w); w) = \text{Dr}$.
3. Calculate $I_{\text{inert}}(w)$ from (4.27).
4. Solve w from (4.28).

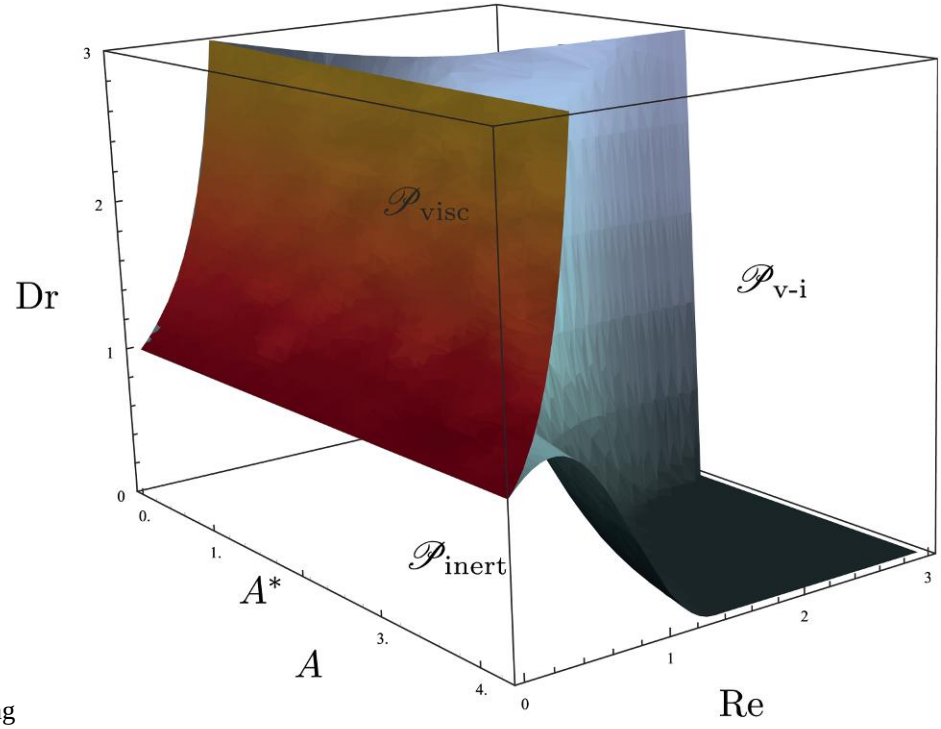

centering

FIG. 4. Parameter regions for three flow regimes $\mathscr{P}_{\text{inert}}$, $\mathscr{P}_{\text{v-i}}$ and $\mathscr{P}_{\text{visc}}$.

The partitioning of the parameter space $\mathscr{P}$ into the regions of inertial $\mathscr{P}_{\text{inert}}$, viscous-inertial $\mathscr{P}_{\text{v-i}}$ and viscous $\mathscr{P}_{\text{visc}}$ jets is presented in Fig. 4. The partitioning follows from the solutions of (4.23–4.26) with the additional condition $\xi(\tau_{\text{end}}) = 0$ for the border between $\mathscr{P}_{\text{v-i}}$ and $\mathscr{P}_{\text{visc}}$, and $\xi(0) = 0$ for the border between $\mathscr{P}_{\text{inert}}$ and $\mathscr{P}_{\text{v-i}}$.

For any set of parameters from $\mathscr{P}_{\text{inert}}$, or $\mathscr{P}_{\text{v-i}}$ or $\mathscr{P}_{\text{visc}}$, a corresponding solution of (4.23–4.26) exists. This solution is unique in the case of viscous-inertial and viscous flow. For the inertial flow, a solution might not be unique when the nozzle does not point vertically down and $\text{Dr} > 1$. In this case up to two solutions exist for an inertial jet and one solution for a viscous or viscous-inertial jet. The questions of existence and uniqueness are fully treated in Hlod (2009, Section 3.6).

In the next section, we justify our choice of the boundary conditions for Θ, i.e. (4.14) and (4.20), for inertial and viscous flow, and we explain why no boundary condition is needed for Θ in case of viscous-inertial flow.

5. Justification of boundary conditions for Θ

In this section, we explain our choice of boundary conditions for Θ made in the previous section. We use the highest-order part, the principal part, of the conservation of momentum equation (3.2)

$$\mathbf{r}_{tt} + 2\upsilon\mathbf{r}_{st} + \upsilon\xi\mathbf{r}_{ss} = [\mathbf{r}_{tt} + 2\upsilon\mathbf{r}_{st} + \upsilon^2\mathbf{r}_{ss}] - \upsilon_s\mathbf{r}_{ss}. \tag{5.1}$$

This equation is of hyperbolic type in the neighbourhood of $s = s_{\text{end}}$, if $\xi(s_{\text{end}})$ is close to zero, and in the neighbourhood of $s = 0$, if $\xi(0)$ is close to zero because $v_s = v^2 + \xi v > 0$ in theses situations. We consider the direction of the characteristics of (5.1), either at $s = s_{\text{end}}$ if $\xi(s_{\text{end}})$ changes sign or at $s = 0$ if $\xi(0)$ changes sign. This directly yields the number of boundary conditions, which must be prescribed at $s = s_{\text{end}}$ or $s = 0$. The reason is that the number of boundary conditions at any point of the boundary is equal to the number of characteristics pointing into the domain at that point; (see Godlewski & Raviart, 1996, p. 417), which follows from the concept of 'domain of dependence' (see Courant & Hilbert, 1989, p. 438–449, for more details).

The characteristic equation (see Davis, 2000, p. 57) for (5.1) is

$$z^2 - 2vz + v^2 - v_s = 0, \tag{5.2}$$

where z is the velocity of a characteristic. Equation (5.2) has the solutions

$$z_1 = v + \sqrt{v_s}, \quad z_2 = v - \sqrt{v_s}. \tag{5.3}$$

According to (5.3) and (3.20), the directions of the characteristics of (5.1) depend on the sign of ξ as follows:

1. If $\xi > 0$ then $z_1 > 0$ and $z_2 > 0$, i.e. both characteristics point to the right.
2. If $\xi = 0$ then $z_1 > 0$ and $z_2 = 0$, i.e. one characteristic points to the right and one is stationary.
3. If $\xi < 0$ then $z_1 > 0$ and $z_2 < 0$, i.e. one characteristic points to the left and one to the right.

From the characterization of the flow regimes (4.11–4.13) we infer that:

- At $s = 0$, two boundary conditions for $\mathbf{r}(s, t)$ are necessary in case of an inertial jet ($\xi(0) > 0$), and only one in case of a viscous-inertial or viscous jet ($\xi(0) \leqslant 0$).
- In case of a viscous jet, one boundary condition for $\mathbf{r}$ is necessary at $s = s_{\text{end}}$ ($\xi(s_{\text{end}}) < 0$), and none in case of viscous-inertial or inertial jets ($\xi(s_{\text{end}}) \geqslant 0$).

For all three situations, we prescribe the nozzle position. In addition, for the inertial jet, the nozzle orientation is prescribed by (4.14), and for the viscous jet, the tangency condition (4.20) with the belt is prescribed. This justifies our choice of boundary conditions (4.14) and (4.20) for the stationary problem.

The analysis of characteristics, as directions of information propagation, explains why the nozzle orientation influences the jet shape only in the case of inertial flow, and why the belt orientation influences the jet shape only in case of viscous flow.

- In inertial flow, all information about the jet shape travels from the nozzle to the belt. Therefore, not only nozzle position but also nozzle orientation is relevant for the jet. In addition, no information on angle travels back from the belt.
- In viscous-inertial flow, only one characteristic (at the nozzle) points inside the domain. Therefore, no information about the nozzle orientation or the belt movement direction influences the jet shape. Thus, in viscous-inertial flow, the nozzle and the belt orientations are irrelevant for the jet.
- In viscous flow, one characteristic points inside the domain at the nozzle and one at the belt. Hence, information about the direction of the belt movement influences the jet shape, and therefore, the belt orientation becomes relevant in viscous flow.

6. Results from the model

In this section, we present some results from this model. We analyse the partitioning of the parameter space. Next, we investigate changes of the flow type if one of the physical parameters (L, ν, v_{belt}, v_{nozzle}) is varied. We describe the trajectories of the process parameters in the parameter space $\mathscr{P}$, and we illustrate the jet shape evolution. Note that the only possible transitions between flow types are between $\mathscr{P}_{\text{inert}}$ and $\mathscr{P}_{\text{v-i}}$, and between $\mathscr{P}_{\text{v-i}}$ and $\mathscr{P}_{\text{visc}}$, as is shown in Fig. 4.

The projection of the regions for the three flow regimes onto the (A, Re)-plane is depicted in Fig. 5, and following is valid for all values of Dr. We observe a region $\{A < A^*, \text{Re} > \mathscr{R}_1(A)\}$ where the jet is inertial, and a region $\{A > A^*, \text{Re} > \mathscr{R}_2(A)\}$ where it is viscous-inertial. In the region between $\mathscr{R}_1$, $\mathscr{R}_2$ and $\mathscr{R}_3$ inertial or viscous-inertial flow is possible but there can be no viscous flow. Finally, in the region $\{A > 0, \text{Re} < \mathscr{R}_3(A)\}$, all three flow regimes are possible. Hence, it is only in the latter region, where $\text{Re} < \mathscr{R}_3(A) < 1$, that a viscous jet can occur.

The parameter regions projection onto the (A, Dr)-plane is depicted in Fig. 6; and the following holds for all Re. We observe that for $\{A > A^*, \text{Dr} < 1\}$ only an inertial jet is possible, while inertial or

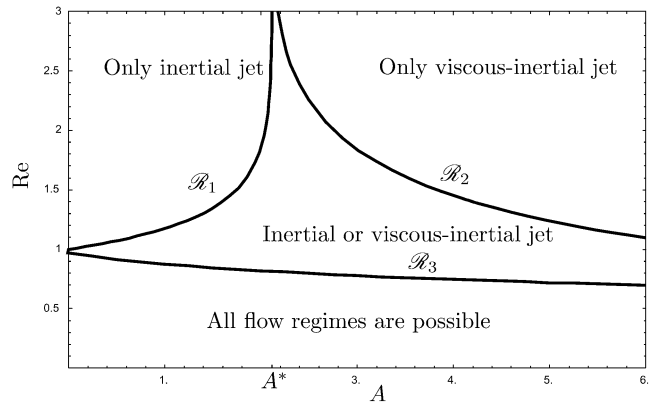

FIG. 5. Regions of A and Re with possible flow regimes for all Dr.

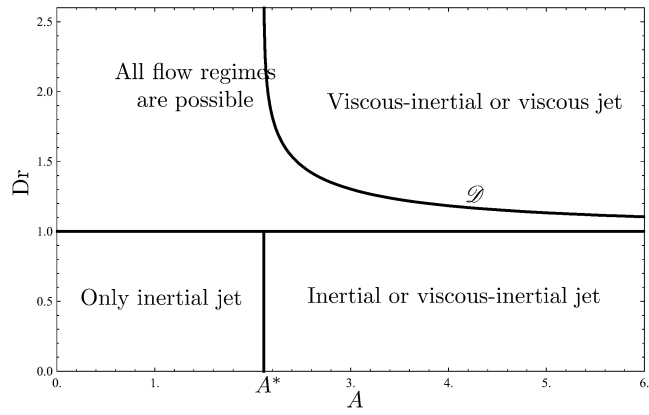

FIG. 6. Regions of A and Dr with possible flow regimes for all Re.

viscous-inertial flow is possible for $\{A > A^*, \mathrm{Dr} < 1\}$. In the region $\{A > A^*, \mathrm{Dr} > \mathscr{D}(A)\}$, viscous or viscous-inertial flow is possible, while in the rest of region $\{\mathrm{Dr} > 1\}$, all three flow regimes are possible. Hence, a viscous jet can only occur if $\mathrm{Dr} > 1$.

Next, we study the change of the jet if one of the physical parameters varies as to change the flow type from viscous to viscous-inertial. For a reference configuration, we take the physical parameters $L = 1\,\mathrm{cm}$, $\nu = 0.047\,\mathrm{m}^2/\mathrm{s}$, $v_{\mathrm{belt}} = 1.4\,\mathrm{m/s}$ and $v_{\mathrm{nozzle}} = 1\,\mathrm{m/s}$, for which the jet is viscous (recall that for the viscous and viscous-inertial flow regimes α_{nozzle} is not relevant). Then, if we increase L, decrease ν, decrease v_{belt}, or increase v_{nozzle}, eventually the jet flow changes from viscous to viscous-inertial. The corresponding curves in the parameter space $\mathscr{P}$ are indicated in Fig. 7.

Changes of the jet shape while only one of the physical parameters L, ν, v_{belt} or v_{nozzle} varies as described above are shown in Fig. 8(a–d), respectively. In Figs 7 and 8, we see that if the point $(A, \mathrm{Re}, \mathrm{Dr})$ approaches the boundary of $\mathscr{P}_{\mathrm{visc}}$, the jet shape becomes vertical. If $(A, \mathrm{Re}, \mathrm{Dr})$ is very close to the boundary of $\mathscr{P}_{\mathrm{visc}}$ the jet shape is almost vertical, except for the small region near the belt where the jet rapidly bends to the horizontal belt direction.

The analysis of the parameter region for the inertial jet is more complex than that for the viscous jet. In case $\{A > A^*,\ \mathrm{Dr} < 1\}$ ('Only inertial jet' in Fig. 6), the flow is inertial for all L. Similar, if $\{A < A^*,\ \mathrm{Re} > \mathscr{R}_1(A)\}$ ('Only inertial jet' in Fig. 5), the flow is inertial for all v_{belt}. In a situation when ν decreases or v_{nozzle} increases, A approaches zero and Re approaches infinity since $A = 3g\nu/v_{\mathrm{nozzle}}^3$, and $\mathrm{Re} = v_{\mathrm{nozzle}}L/(3\nu)$. Thus, eventually the point (A, Re) enters the 'Only inertial jet' region in Fig. 5. Hence, if the jet is not in the inertial flow regime, decreasing ν or increasing v_{nozzle} makes the jet to become inertial eventually.

To illustrate the change of flow from inertial to viscous-inertial, while only one of the parameters L, ν, v_{belt} and v_{nozzle} varies, we take the reference values $L = 30\,\mathrm{cm}$, $\nu = 0.2\,\mathrm{m}^2/\mathrm{s}$, $v_{\mathrm{belt}} = 2\,\mathrm{m/s}$ and $v_{\mathrm{nozzle}} = 1.5\,\mathrm{m/s}$. Then, if we decrease L, increase ν, increase v_{belt} or decrease v_{nozzle} eventually the jet flow changes from inertial to viscous-inertial. The curves in the parameter space $\mathscr{P}$ are indicated in Fig. 9.

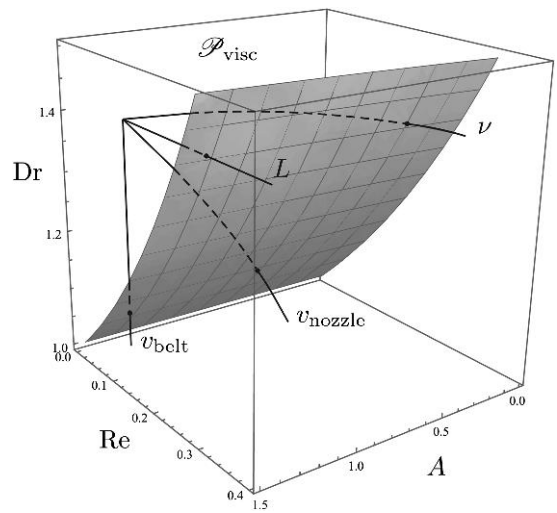

FIG. 7. Traces of the point $(A, \mathrm{Re}, \mathrm{Dr})$ as we change one of the physical parameters (L increases, ν decreases, v_{belt} decreases, v_{nozzle} increases). The curves originate at the same point in the region $\mathscr{P}_{\mathrm{visc}}$ and eventually leave $\mathscr{P}_{\mathrm{visc}}$ by crossing the separating grey surface at the points indicated by the dots.

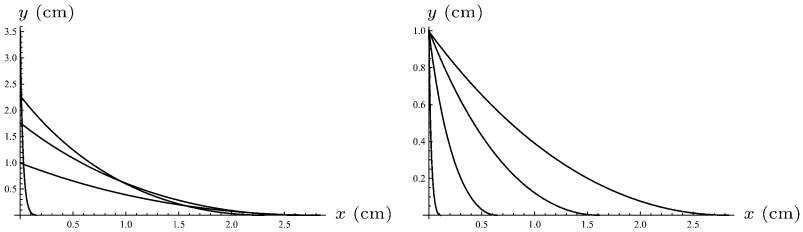

(a) Viscous jet shapes for different L: 1, 1.7, 2.2, and 3.5 cm. The shape approaches the vertical as L increases.

(b) Viscous jet shapes for different ν: 0.047, 0.026, 0.015, and 0.012 m^2/s. The shape approaches the vertical as ν decreases.

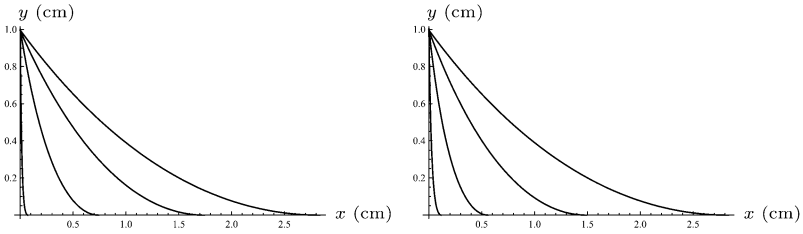

(c) Viscous jet shapes for different v_{belt}: 1.4, 1.21, 1.11, and 1.08 m/s. The shape approaches the vertical as v_{belt} decreases.

(d) Viscous jet shapes for different v_{nozzle}: 1, 1.16, 1.24, and 1.26 m/s. The shape approaches the vertical as v_{nozzle} increases.

FIG. 8. Convex shapes of the viscous jet for different values of L, ν, v_{belt} and v_{nozzle}. The reference values are $L = 1\,\text{cm}$, $\nu = 0.047\text{m}^2/\text{s}$, $v_{\text{belt}} = 1.4\,\text{m/s}$ and $v_{\text{nozzle}} = 1\,\text{m/s}$.

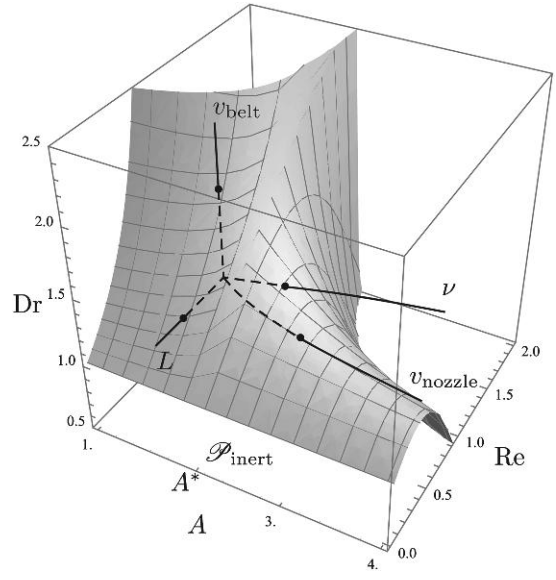

FIG. 9. Curves in the parameter space $\mathscr{P}$ as we change one of the parameters (L decreases, ν increases, v_{belt} increases, v_{nozzle} decreases). The curves originates at the same point in the region $\mathscr{P}_{\text{inert}}$ and eventually leave $\mathscr{P}_{\text{inert}}$ by crossing the separating surface at the points indicated by the dots.

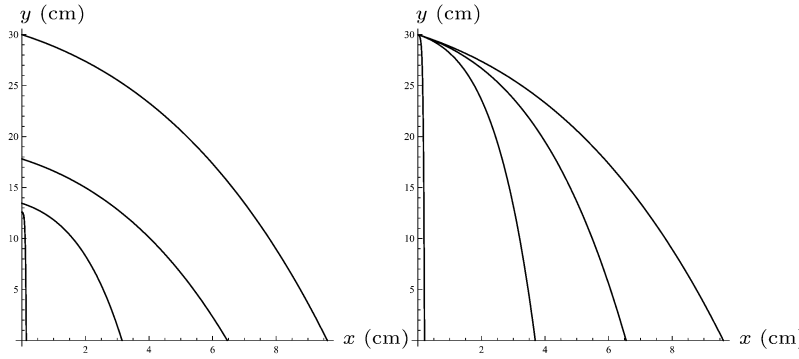

(a) Inertial jet shapes for different L: 30, 18, 13, and 12 cm. The shape approaches the vertical as L decreases.

(b) Inertial jet shapes for different ν: 0.2, 0.26, 0.3, and 0.32 m^2/s. The shape approaches the vertical as ν increases.

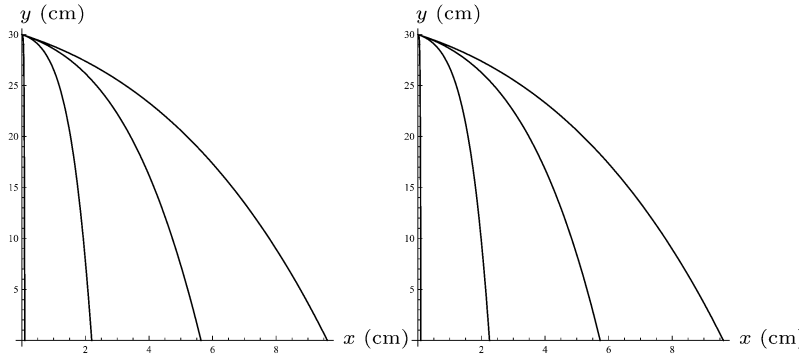

(c) Inertial jet shapes for different v_{belt}: 2, 2.57, 2.86, and 2.95 m/s. The shape approaches the vertical as v_{belt} increases

(d) Inertial jet shapes for different v_{nozzle}: 1.5, 1.4, 1.36, and 1.34 m/s. The shape approaches the vertical as v_{nozzle} decreases.

FIG. 10. Concave shapes of the inertial jet for different values of L, ν, v_{belt}, v_{nozzle}. The reference values are $L = 30\,\mathrm{cm}$, $\nu = 0.2\,\mathrm{m}^2/\mathrm{s}$, $v_{\mathrm{belt}} = 2\,\mathrm{m/s}$ and $v_{\mathrm{nozzle}} = 1.5\,\mathrm{m/s}$. The nozzle orientation is $\alpha_{\mathrm{nozzle}} = \pi/4$.

Changes of the jet shape for $\alpha_{\mathrm{nozzle}} = \pi/4$, while only one of the physical parameters L, ν, v_{belt}, or v_{nozzle} varies as described above are shown in Fig. 10(a–d), respectively. In Figs 9 and 10, we see that if the point $(A, \mathrm{Re}, \mathrm{Dr})$ approaches the boundary of $\mathscr{P}_{\mathrm{inert}}$, the jet shape becomes more vertical. If $(A, \mathrm{Re}, \mathrm{Dr})$ is very close to the boundary of $\mathscr{P}_{\mathrm{inert}}$ the jet shape is almost vertical except for the small region near the belt where the jet rapidly bends from the nozzle direction to an almost vertical one.

The analysis above shows that the transition between the viscous and the inertial flow regimes as parameters continuously vary is only possible via the viscous-inertial flow.

7. Experiments

In this section, we describe experiments of the fall of a thin jet onto a moving belt. The main goal of these experiments is to confirm the existence of the three flow regimes and the position, as a function

of v_{belt}, of the interfaces between them. Two values of v_{nozzle}, L, d_{nozzle} and α_{nozzle} are used for two sequences of experiments. In each sequence, v_{belt} is allowed to vary. For the details of these and other experiments, we refer to Hlod (2009).

A viscous fluid, polybutene Indopol H-100, is pumped to a nozzle and allowed to fall from the nozzle onto a moving belt (see Fig. 3). The belt is wrapped around two parallel cylinders so that the belt is horizontal. The left cylinder is connected to an electric motor to move the belt from the left to the right with a constant speed.

The nozzle is placed above the belt. A screw pump producing a constant flow rate is connected to the nozzle. The flow rate was measured by weighing the fluid collected from the nozzle during 30 s. In the experiments, two different nozzles were used, with diameters of 1 mm and 0.4 mm. The experimental setup allows us to change the nozzle position and orientation, belt velocity and nozzle flow velocity. The parameter values of the two sequences of experiments are given in Table 1.

First, we describe a typical sequence of experiments. We start with v_{belt} close to zero and make sure that L and v_{nozzle} are chosen such that the shape of the jet is concave resembling a ballistic trajectory (see Fig. 1(a)). To obtain the concave jet shape, the nozzle should not point down vertically, and therefore we put $\alpha_{\text{nozzle}} < \pi/2$. Next, we gradually increase v_{belt} and study the evolution of the jet shape.

For small v_{belt}, the jet shape is concave with an unsteady region near the belt (see Fig. 1(a)). By increasing v_{belt}, we observe that the unsteady region near the belt transforms into a stable bending region where the jet bends to the horizontal belt direction (see Fig. 1(b)). The jet shape in this region resembles the backward-pointing heel, reported for the vertically falling jet in Chiu-Webster & Lister (2006).

When we increase v_{belt} further, the jet shape approaches the vertical direction. In this case, the contact point with the belt approaches the vertical projection of the nozzle position. As a result, for v_{belt} large enough, the main part of the jet between the belt and the nozzle is purely vertical (see Fig. 1(c)). The bending region near the belt remains, and a new bending region near the nozzle appears. Near the nozzle, the jet bends from the nozzle orientation to the vertical direction.

Further increase in v_{belt} results in the disappearing of the local region near the belt, where the jet bends from the vertical to the horizontal belt direction. The jet shape becomes convex everywhere, except for a bending region near the nozzle (see Fig. 1(d)). The touchdown point moves away from the nozzle in the direction of the belt motion as v_{belt} increases.

Summarizing the results of the experiments, we observe a concave jet shape for small v_{belt}, except

TABLE 1 *Values of the experimental parameters*

Parameter name		Sequence 1	Sequence 2	Units
Belt velocity	v_{belt}	0.100–5.622	0.093–3.200	m/s
Flow velocity at nozzle	v_{nozzle}	1.147	1.061	m/s
Distance between belt and nozzle	L	0.041	0.054	m
Nozzle orientation†	α_{nozzle}	5°	37.3°	
Kinematic viscosity of fluid	ν	0.047	0.047	m^2/s
Fluid density	ρ	880	880	kg/m^3
Nozzle diameter	d_{nozzle}	0.4	1	mm

†The angle between the nozzle orientation and the horizontal direction, positive for downwards-pointing nozzle.

for a small bending or unstable region near the belt. With increasing v_{belt}, the jet shape becomes vertical, except for small bending regions near the nozzle and the belt. Further increase of v_{belt} leads to a convex jet shape, except for a small bending region near the nozzle. This gives a characterization of the jet flow by its shape, i.e. concave, vertical and convex, which, as it was shown in Section 3, is related to the characterization based on the dominant effect in the momentum transfer through the jet cross section, i.e. inertial, viscous-inertial and viscous, respectively.

A convenient way to quantify the jet behaviour is by the horizontal position x_{end} of the touchdown point at the belt. For the jet with small v_{belt}, the contact point is away from the nozzle in the direction of the nozzle. With increasing v_{belt}, the touchdown point moves first towards the nozzle position (x_{end} decreases) until the jet becomes vertical ($x_{\text{end}} = 0$), stays vertical for some range of values of v_{belt} and then moves away from the nozzle position in the direction of the belt motion (x_{end} increases).

Figure 11 shows this dependence of x_{end} on v_{belt}. The graph suggests that the first five dots are in the inertial flow regime, the sixth, with $x_{\text{end}} = 0$, represents a viscous-inertial flow, and the remaining ones (7th and higher) are in the viscous flow regime. Thus, this corresponds to the regions of v_{belt} predicted by the model.

A comparison between the theoretical predictions of x_{end} and the one from experiments is depicted in Fig. 12 and shows a mismatch for the jets in inertial and viscous regimes. The model predicts x_{end}, on average, three times larger than obtained experimentally.

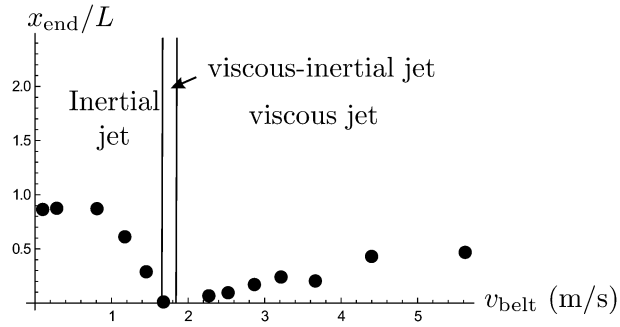

FIG. 11. Positions of the touchdown point x_{end} for different v_{belt} indicated by •, obtained from Sequence 1. The vertical lines indicate the model predictions of regions of v_{belt} for the three flow regimes.

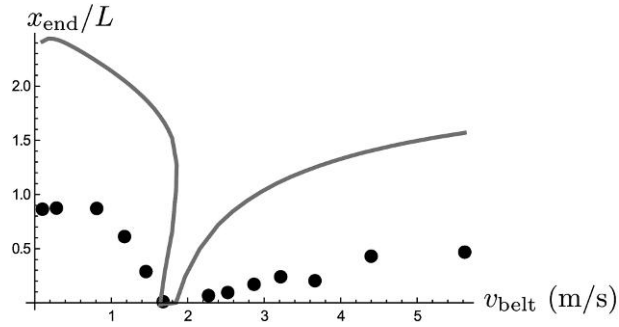

FIG. 12. Comparison of the relations between v_{belt} and x_{end} as obtained from the model (solid grey line), and from Sequence 1.

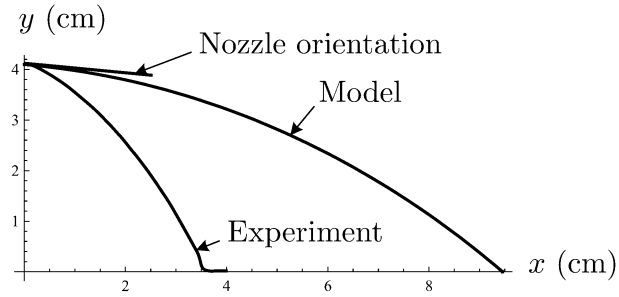

FIG. 13. Comparison of the inertial jet shapes obtained theoretically and experimentally for Sequence 1 and $v_{\text{belt}} = 0.81\,\text{m/s}$.

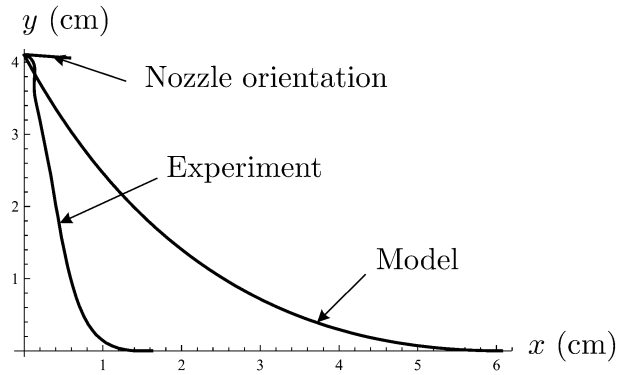

FIG. 14. Comparison of the viscous jet shapes obtained theoretically and experimentally for Sequence 1 and $v_{\text{belt}} = 4.398\,\text{m/s}$.

We look for the cause of these differences in the effects which we did not include in our model, such as air drag, bending stiffness and surface tension.

We use the model with surface tension from Chiu-Webster & Lister (2006). The surface tension coefficient is $0.027\,\text{N/m}$. The jets in the inertial and viscous regimes, obtained from the model with surface tension, do not show better agreement with the experiments (see Fig. 15(a and b). Including the effect of surface tensions to the model gives a slightly smaller x_{end} and the overall inertia and viscous jet shapes differ very little.

Using the model with bending stiffness from Ribe *et al.* (2006) for the jets in inertial and viscous regimes, we obtain shapes similar to those from our model besides small bending regions at the belt in the inertial regime and at the nozzle in the viscous regime. However, the overall shape of the jets does not explain the difference with the experimental ones (see Fig. 16(a and b). The effect of bending stiffness does not make any significant difference for the inertia jet and produces smaller x_{end} for the viscous jet.

The model with air drag from Yarin (1993, p. 54) also does not explain the differences in jet shapes (see Figs 17 and 18). The air drag is modelled by adding the term

$$-\frac{1}{2}C_N \rho_{\text{air}} v^2 \pi \, \mathrm{d}\mathbf{r}_s,$$

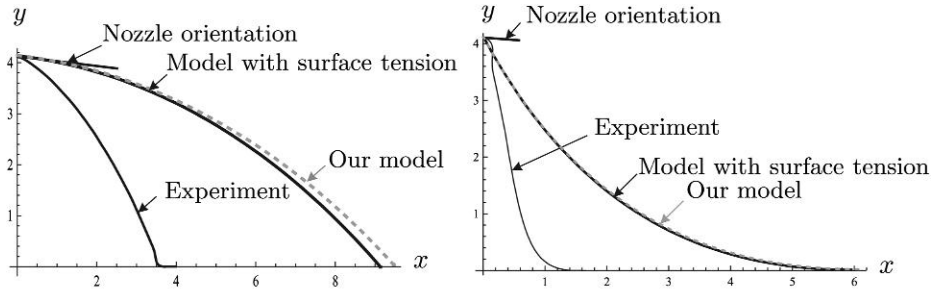

(a) Inertial jet with $v_{\text{belt}} = 0.81\,\text{m/s}$ (b) Viscous jet with $v_{\text{belt}} = 4.398\,\text{m/s}$

FIG. 15. The jet shapes from the model with surface tension, from our model (grey, dashed line) and from the experiments from Sequence 1.

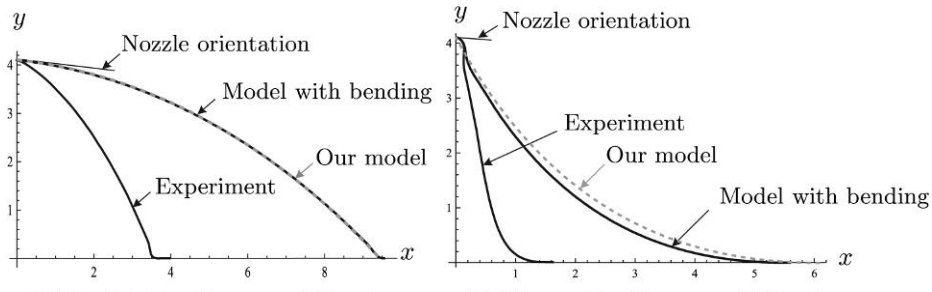

(a) Inertial jet with $v_{\text{belt}} = 0.81\,\text{m/s}$ (b) Viscous jet with $v_{\text{belt}} = 4.398\,\text{m/s}$

FIG. 16. The jet shapes from the model with bending stiffness, from our model (grey, dashed line) and from the experiments from Sequence 1.

to the right-hand side of the conservation of momentum (3.2). Here, ρ_{air} is the air density, C_N is the drag coefficient and d is the jet diameter. The value C_N is usually obtained heuristically; see, for example, Salamone, 1996, p. 4070 and Nakajima *et al.*, 1994, p. 43. To illustrate the influence of the air drag we present the jet shapes for several values of C_N. For small values of C_N, the jet shape remains concave for the inertial jet and convex for the viscous jet (see Figs 17 and 18). With increasing C_N for the viscous and inertial jets, the inertia starts to dominate at the nozzle and viscosity at the belt, so the jet becomes aligned with the nozzle and concave near the nozzle, and convex near the belt. At the point where $\xi = 0$ the jet is vertical. However, changing C_N does not provide us with a better fit between the jet shapes obtained from the model with air drag and from the experiments.

We conclude that our experiments confirm the existence of the three flow regimes and the positions of the interfaces that we found analytically. In this respect, these experiments can be seen as a proof of principle for our choice of boundary conditions for each regime. However, a comparison between the jet shapes computed with our model and those found experimentally has shown a quantitative difference between our model predictions and the experiments for the jets in the viscous and inertial regimes. Including effects of surface tension, air drag or bending stiffness alone does not explain the difference between the jet shapes obtained theoretically and experimentally.

To improve the agreement between the model and the experiment, we propose to change the experimental setup and include more effects in the model. Experiments should be done with different fluids

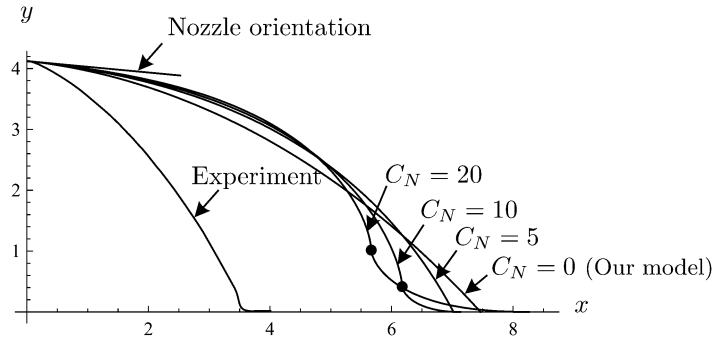

FIG. 17. The inertial jet shapes obtained from the model with air drag and from the experiment from Sequence 1 and $v_{\text{belt}} = 0.81\,\text{m/s}$. The dimensionless drag coefficient C_N has values 0, 5, 10 and 20. The solid dots indicate the positions in which $\xi = 0$ and the jets are vertical.

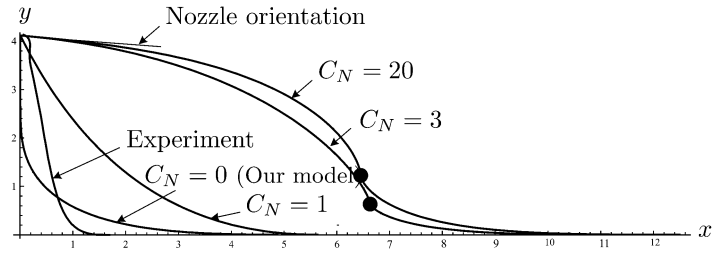

FIG. 18. The viscous jet shapes obtained from the model with air drag and from the experiment Sequence 1 and $v_{\text{belt}} = 4.398\,\text{m/s}$. The dimensionless drag coefficient C_N has values 0, 1, 3 and 20. The solid dots indicate the positions in which $\xi = 0$ and the jets are vertical.

with varying viscosity. Measuring airflow and/or using air baffles would be of additional improvement. The model could be improved by considering a viscoelastic constitutive law for the fluid and including a transversal air flow.

8. Summary of the three flow regimes

Using our knowledge about the three flow regimes from the model and the experiments, we describe typical features of each flow regime. In the model, the three flow regimes are characterized by the sign of the dimensionless variable ξ. The value of ξ represents the momentum transfer through a cross section of the jet and describes the balance between the inertia and viscous terms in the conservation of momentum equation (3.5). Flow characterization using experimental jet shape features is possible as well. Below, we describe each flow regime separately

- Inertial flow. In this flow regime, ξ is positive. This means that the momentum transfer due to inertia is larger than that due to viscosity. This is reflected in the concave shape (disregarding a small bending or unsteady region near the belt) of the jet comparable to a ballistic trajectory and aligned with the nozzle orientation.
- Viscous-inertial flow. In this flow regime, ξ changes sign from negative near the nozzle to positive near the belt. Hence, the momentum transfer due to viscosity is larger near the nozzle and the one

due to inertia is so near the belt. The belt and nozzle orientations are now irrelevant for the jet shape, which is straight vertical in the experiments (except a possible bending region near the nozzle and bending or unstable region near the belt) as well as in the model.

- **Viscous flow.** In this flow regime, ξ is negative, which means that the momentum transfer due to viscosity is larger than that due to inertia. Both in the experiments and the model the jet shape is convex (disregarding a small bending region near the nozzle in the experiment) and the jet touches the belt tangentially.

Summarizing, we conclude that the flow regimes can be characterized by the sign of the momentum transfer through the cross section of the jet or by the convexity of the jet shape. However, for $\alpha_{\text{nozzle}} = \pi/2$, the inertial jet shape is vertical, which makes it then impossible to distinguish between the inertial and viscous-inertial flow regimes. Moreover, other shape features such as the tangency condition at the belt for the viscous flow, and the relevance of the nozzle orientation for the inertial flow can be used to distinguish these flow regimes.

9. Conclusions and discussion

In this paper, we have studied the problem of the fall of a jet of viscous fluid onto a moving belt. Three flow regimes of the jet are distinguished and characterized by the dominant effect in the momentum transfer through a cross section of the jet, i.e. inertial, viscous-inertial and viscous.

We have modelled the jet using a thin-jet approximation (string model) including the effects of inertia, viscous tension and gravity. The model consists of the stationary conservation laws for mass and momentum. A change of the independent variable is made to allow for a transformation of the model equations into an algebraic equation. The partitioning of the parameter space between the three flow regimes is evaluated in terms of three dimensionless numbers.

The model shows that the sign of the momentum transfer through a cross section of the jet determines the corresponding flow regime. For each flow regime, the correct boundary condition for the jet orientation is derived by looking at the characteristics of the dynamic conservation of momentum equation. These boundary conditions for the jet orientation are

1. the nozzle orientation for the inertial jet,
2. no boundary condition for the viscous-inertial jet,
3. the tangency of the jet at the belt for the viscous jet.

The missing boundary condition for the viscous-inertial jet is replaced by the constraint that at the point where the momentum transfer equals zero the jet is aligned with the vertical direction of gravity.

It is shown that a continuous transition between the inertial and the viscous jets is only possible via the viscous-inertial one. Also the way how the dimensional parameters should be changed in order to leave the viscous or inertial jet region is indicated.

Experimental results for the positions of the touchdown points as a function of v_{belt} prove the existence of three regimes and the experimentally obtained positions of the interfaces between these regimes correspond to those obtained analytically. The jet shape comparison reveals a significant difference between the theory and the experiments. Including surface tension, air drag or bending stiffness in the model does not explain the difference.

Acknowledgements

The authors would like to acknowledge Teijin Aramid, a part of the Teijin group of companies for providing the experimental equipment and valuable suggestions for experiments.

REFERENCES

ADACHI, K. (1987) Laminar jets of a plane liquid sheet falling vertically in the atmosphere. *J. Nonnewton Fluid Mech.*, **24**, 11–30.

CHIU-WEBSTER, S. & LISTER, J. R. (2006) The fall of a viscous thread onto a moving surface: a 'fluid-mechanical sewing machine'. *J. Fluid Mech.*, **569**, 89–111.

CLARKE, N. S. (1966) A differential equation in fluid mechanics. *Mathematika*, **13**, 51–53.

CLARKE, N. S. (1968) Two-dimensional flow under gravity in a jet of viscous liquid. *J. Fluid Mech.*, **31**, 481–500.

COURANT, R. & HILBERT, D. (1989) *Methods of Mathematical Physics*. vol. II. New York: Wiley Classics Library. John Wiley & Sons Inc. Partial differential equations, Reprint of the 1962 original, A Wiley-Interscience Publication.

CRUICKSHANK, J. O. (1980) Viscous fluid buckling: a theoretical and experimental analysis with extensions to general fluid stability. *Ph.D. Thesis*, Iowa State University, Ames, IA.

DAVIS, J. L. (2000) *Mathematics of Wave Propagation*. Princeton, NJ: Princeton University Press.

DECENT, S. P., KING, A. C. & WALLWORK, I. M. (2002) Free jets spun from a prilling tower. *J. Eng. Math.*, **42**, 265–282.

DEN DECKER, P., KNOESTER, H., MEERMAN, H., DEKKER, W., VAN HORSSEN, K., VUIK, C., WESSELING, P., PROKERT, G., VAN 'T HOF, B. & VAN BECKUM, F. (2004) The rotor spinning process for fibre production. P*roceedings of the 48th European Study Group Mathematics with Industry* (C. Kraaikamp, H. X. Lin & C. W. Oosterlee eds). Delft, The Netherlands: Delft University Press, pp. 35–48.

DYSON, R. J., HOWELL, P. D., BREWARD, C. J. W., HERDMAN, P. & BRANDER, J. (2005) Mathematical modelling of curtain coating. *Proceedings of the 6th European Coating Symposium ECS2005*. Preprint available at http://eprints.maths.ox.ac.uk/234/1/ECSrjdpaper.pdf.

ENTOV, V. M. & YARIN, A. L. (1980) Dynamical equation for a liquid jet. *Trans. Izvestiya Akademii Nauk SSSR Mekhanika Zhidkosti i Gaza*, **5**, 11–18.

GODLEWSKI, E. & RAVIART, P.-A. (1996) *Numerical Approximation of Hyperbolic Systems of Conservation Laws*. Applied Mathematical Sciences, vol. 118. New York: Springer.

GÖTZ, T., KLAR, A., UNTERREITER, A. & WEGENER, R. (2008) Numerical evidence for the non-existence of stationary solutions of the equations describing rotational fiber spinning. *Math. Model Methods Appl. Sci.*, **18**, 1829–1844.

HLOD, A. (2009) Curved jets of viscous fluid: interactions with a moving wall. *Ph.D. Thesis*, Eindhoven University of Technology, Eindhoven, The Netherlands.

HLOD, A., AARTS, A. C. T., VAN DE VEN, A. A. F. & PELETIER, M. A. (2007) Mathematical model of falling of a viscous jet onto a moving surface. *Eur. J. Appl. Math.*, **18**, 659–677.

KOLK, E. (2005) Mathematical models for a rotor spinning process. *Interim Report*, Delft, The Netherlands: TU Delft.

MARHEINEKE, N. & WEGENER, R. (2009) Asymptotic model for the dynamics of curved viscous fibres with surface tension. *J. Fluid Mech.*, **622**, 345–369.

MARSTON, J. O., DECENT, S. P. & SIMMONS, M. J. H. (2006) Hysteresis and non-uniqueness in the speed of the onset of instability in curtain coating. *J. Fluid Mech.*, **569**, 349–363.

MARSTON, J. O., DECENT, S. P. & SIMMONS, M. J. H. (2008) Experimental evidence of non-unique solutions to a steady non-linear coating flow. *IMA J. Appl. Math.*, **73**, 698–702.

MORRIS, S. W., DAWES, J. H. P., RIBE, N. M. & LISTER, J. R. (2008) Meandering instability of a viscous thread. *Phys. Rev. E Stat. Nonlinear Softw Matter Phys.*, **77**, 066–218.

NAKAJIMA, T., KAJIWARA, K. & MCINTYRE, J. E. (1994) *Advanced Fiber Spinning Technology*. Cambridge: Woodhead Publishing.

PANDA, S. (2006) The Dynamics of viscous fibers. *Ph.D. Thesis*, Technische Universität Kaiserslautern, Kaiserslautern, Germany.

PANDA, S., MARHEINEKE, N. & WEGENER, R. (2008) Systematic derivation of an asymptotic model for the dynamics of curved viscous fibers. *Math. Methods Appl. Sci.*, **31**, 1153–1173.

PARAU, E. I., DECENT, S. P., KING, A. C., SIMMONS, M. J. H. & WONG, D. C. (2006) Nonlinear travelling waves on a spiralling liquid jet. *Wave Motion*, **43**, 599–618.

PARAU, E. I., DECENT, S. P., SIMMONS, M. J. H., WONG, D. C. Y. & KING, A. C. (2007) Nonlinear viscous liquid jets from a rotating orifice. *J. Eng. Math.*, **57**, 159–179.

PARTRIDGE, L., WONG, D. C. Y., SIMMONS, M. J. H., PARAU, E. I. & DECENT, S. P. (2005) Experimental and theoretical description of the break-up of curved liquid jets in the prilling process. *Chem. Eng. Res. Des.*, **83**, 1267–1275.

RIBE, N. M. (2003) Periodic folding of viscous sheets. *Phys. Rev. E*, **68**, 036–305.

RIBE, N. M. (2004) Coiling of viscous jets. *Proc. R. Soc. Lond. A*, **460**, 3223–3239.

RIBE, N. M., LISTER, J. R. & CHIU-WEBSTER, S. (2006) Stability of a dragged viscous thread: onset of stitching in a fluid-mechanical sewing machine. *Phys. Fluids*, **18**, 124105–124113.

ROOS, J. P., SCHWEIGMAN, C. & TIMMAN, R. (1973) Mathematical formulation of the laws of conservation of mass and energy and the equation of motion for a moving thread. *J. Eng. Math.*, **7**, 139–146.

SALAMONE, J. C. (1996) *Polymeric Materials Encyclopedia*. Boca Raton, FL: CRC Press.

SAUTER, U. S. & BUGGISCH, H. W. (2005) Stability of initially slow viscous jets driven by gravity. *J. Fluid Mech.*, **533**, 237–257.

SKOROBOGATIY, M. & MAHADEVAN, L. (2000) Folding of viscous sheets and filaments. *Europhys. Lett.*, **52**, 532–538.

TAYLOR, G. I. (1969) Instability of jets, threads, and sheets of viscous fluid. *Proceedings of the 12th International Congress of Applied mechanics Stanford, 1968* (M. Het'enyi & W. G. Vincenti eds). Stanford: Springer, pp. 382–388.

TCHAVDAROV, B. M., YARIN, A. L. & RADEV, S. (1993) Buckling of thin liquid jets. *J. Fluid Mech.*, **253**, 593–615.

UDDIN, J., DECENT, S. P. & SIMMONS, M. J. (2006) The instability of shear thinning and shear thickening spiralling liquid jets: linear theory. *Trans. ASME J. Fluids Eng.*, **128**, 968–975.

WALLWORK, I. M., DECENT, S. P., KING, A. C. & SCHULKES, R. M. S. M. (2002) The trajectory and stability of a spiralling liquid jet. part 1. inviscid theory. *J. Fluid Mech.*, **459**, 43–66.

WONG, D. C. Y., SIMMONS, M. J. H., DECENT, S. P., PARAU, E. I. & KING, A. C. (2004) Break-up dynamics and drop size distributions created from spiralling liquid jets. *Int. J. Multiphas. Flow*, **30**, 499–520.

YARIN, A. L. (1993) *Free Liquid Jets and Films: Hydrodynamics and Rheology*. Interaction of Mechanics and Mathematics Series. Harlow: Longman Scientific & Technical.

YARIN, A. L. & TCHAVDAROV, B. M. (1996) Onset of folding in plane liquid films. *J. Fluid Mech.*, **307**, 85–99.